



Ni-Co bimetallic catalysts for the simultaneous production of carbon nanofibres and syngas through biogas decomposition

J.L. Pinilla ^{*}, S. de Llobet, R. Moliner, I. Suelves

Instituto de Carboquímica, CSIC, C/Miguel Luesma 4, 50018 Zaragoza, Spain



ARTICLE INFO

Article history:

Received 29 April 2016

Received in revised form 30 June 2016

Accepted 14 July 2016

Available online 15 July 2016

Keywords:

Biogas

Synthesis gas

Carbon nanofibers

NiCo bimetallic

Catalysts

Decomposition

ABSTRACT

Catalytic Decomposition of Biogas (CDB) is proposed to obtain bio-based materials from biogas in form of valuable carbon nanofilaments together with a syngas in a typical ratio close to 1. NiCo bimetallic catalysts with different Ni/Co ratio were studied in the CDB at different reaction temperatures and WHSV, and the results were related to the catalyst characterization and to the type of carbon formed during reaction. Bimetallic catalyst with an equimolar Ni/Co composition showed the highest carbon yield and sustainability factor at 700 °C and 120 L_N g_{cat}⁻¹ h⁻¹. However, if we attend to the carbon efficiency, lower temperatures and WHSV favour carbon formation. Its good performance was related to a synergistic effect between Ni and Co: the presence of Ni favoured surface carbon diffusion while the presence of Co favoured soot and carbon particles oxidation via redox. The combination of both effects allows that the NiCo-33.5-r catalyst was able to produce an important amount of carbon nanofilaments maintaining good catalyst stability.

© 2016 Elsevier B.V. All rights reserved.

1. Introduction

Biogas is a renewable energy source composed mainly by CH₄ and CO₂ produced from the anaerobic digestion of the organic matter (agricultural wastes, landfills, urban and industrial wastewater). Traditionally, biogas has been considered a non-value by-product which was generally burned in flares to prevent human and environmental risks and then released into the atmosphere as CO₂. Most recently, different alternatives for biogas utilization have been proposed such as the generation of heat, electricity, combined heat and power or bio-methane production that can be used as feedstock in different processes [1]. Another interesting option is the production of synthesis gas (syngas), which is composed by a mixture of H₂ and CO and constitutes the base of the C1 chemistry [2]. Among the different processes by which syngas can be obtained from biogas, dry reforming of methane (DRM) is the most promising one due to the presence of both methane and carbon dioxide in biogas. One of the most important challenges of DRM is the deactivation of the catalysts due to the formation of carbon during CH₄ decomposition and CO₂ disproportionation reactions [3–5]. Problems associated with carbon deposition are even of more significance when biogas is used [6]. Biogas gener-

ally presents CH₄:CO₂ ratios higher than one, eventually provoking larger amount of carbon depositions that rapidly deactivate the catalysts. However, during hydrocarbons decomposition, different kinds of carbon are formed and not all of them are directly responsible of catalyst deactivation [7–10]. According to Menon et al. [11], the kind and location of carbon atoms are more important than the amount produced when catalytic activity is considered. Generally, only encapsulating carbon is directly responsible of catalyst deactivation due to the covering of the active centres, while other carbon structures, such as carbon nanofilaments, only cause operating problems when they are produced in large quantities since reactor blockage can take place. These problems can be avoided by using a suitable reactor configuration, such a fluidized bed reactor [12]. Carbon nanofilaments, including carbon nanofibers (CNF) and carbon nanotubes (CNT), are filaments with diameters ranging from 1 to 200 nm and lengths of several micrometres formed by the stack of graphene layers and classified by their orientation. Carbon nanofilaments have attracted the interest of the scientific community due to their unique properties [13]. Among them, high thermal and electricity conductivity and interesting textural properties make them a promising material in a number of research areas such as catalysis [14,15], energy storage [16] or additive in polymer composites [17]. The synthesis of these materials from a renewable source such as biogas instead of other non-renewable feedstocks typically used would allow them to be classified as bio-based materials.

* Corresponding author.

E-mail address: jlpinilla@icb.csic.es (J.L. Pinilla).

Taking advantage of the possibility of obtaining bio-based materials from biogas in form of valuable carbon nanofilaments together with a syngas in a typical ratio close to 1, a process named Catalytic Decomposition of Biogas (CDB) was recently proposed by our research group [6]. Previous studies focused on the influence of the process variables (space velocity, temperature, CH₄/CO₂ partial pressures) [18,19] using a massive Ni/Al₂O₃, which allowed to establish the optimum conditions to obtain high CH₄ conversions and carbon in form of fishbone-like CNF avoiding catalyst deactivation. The use of different active phases such as Fe and Co revealed the formation of different carbon structures (parallel and chain-like CNF), although catalytic performance in terms of methane conversion and filamentous carbon yield was significantly lower as compared to the Ni based catalysts mainly due to the formation of encapsulating carbon [20].

The utilization of bimetallic catalysts in the dry reforming of CH₄ has been extensively studied during the last years [21,22]. The promising results obtained have been related to a synergistic effect between the two metals [23–25] that leads to a better dispersion and reduction of the active phase and to the modification of the physicochemical properties of the resulting catalyst due to the formation of a solid solution. In particular, it has been reported that NiCo bimetallic catalysts presented higher cooking rates in the DRM than a Co monometallic catalyst [23]. Since the aim of CDB is to obtain high carbon yields, in this work we focused on the performance of NiCo bimetallic catalysts. Their catalytic performance in the CDB was analyzed considering CH₄ and CO₂ conversions, reaction rates, catalyst stability and carbon yield. Additionally, the CNF produced were characterized by transmission electron microscopy (TEM) in order to address the effect of the variation of the Ni/Co ratio.

2. Experimental

2.1. Catalysts synthesis

Three bimetallic catalysts were synthesized by the fusion method, previously described in [26], employing Ni(NO₃)₂·6H₂O, Co(NO₃)₂·6H₂O and Al(NO₃)₃·9H₂O as precursors. Ni and Co act as active phases (AP) and Al₂O₃ as textural promoter. The AP:Al molar ratio was kept at 67:33 and the Ni:Co molar ratio was varied, resulting in three different Ni:Co:Al molar ratios, namely: 50:17:33, 33.5:33.5:33 and 17:50:33. Catalysts are denoted as NiCo-X-s, where "X" refers to the total Ni molar content (50, 33.5 or 17%) and the suffix "s" to the catalyst state: calcined ("c") or reduced ("r"). Thus, NiCo-50-r corresponds to the reduced bimetallic catalyst with a Ni:Co:Al molar ratio of 50:17:33. Additionally, two monometallic catalysts were synthesized by the same method but employing Ni or Co alone as active phase for comparison purposes. These catalysts present a AP:Al molar ratio of 67:33 and are named Ni-67-s and Co-67-s.

2.2. Experimental procedure

To carry out the experiments, a synthetic CH₄:CO₂ mixture with a volume ratio of 60:40 was used. This volume ratio was chosen in order to mimic biogas composition. Catalytic experiments were carried out in a fixed-bed quartz reactor, 15 mm i.d., 750 mm height, fed by the top and heated by an electric furnace. A Peltier cooler was placed after the reactor to condense steam formed during the reaction. Tests were performed at a reaction temperature of 700 °C and a weight hourly space velocity (WHSV, defined here as the total flow rate at normal conditions per gram of catalyst initially loaded) of 120 L_N g_{cat}⁻¹ h⁻¹. Before each test, 0.05 g of oxidized catalyst were loaded in the reactor and in-situ reduced with a H₂ flow

of 100 mL min⁻¹ for 1 h. Different reduction temperatures were chosen for each catalyst according to experimental data and TPR analysis: 550 °C for Ni-67-c and NiCo-50-c, 600 °C for NiCo-33.5-c and 650 °C for NiCo-17-c and Co-67-c. Then, a synthetic biogas flow rate of 100 mL min⁻¹ was fed into the reactor for 3 h. Additional experiments were carried out at 600 and 700 °C and 30 L_N g_{cat}⁻¹ h⁻¹ with the NiCo-33.5-c and monometallic catalysts.

CH₄ conversions, X_{CH4,t} (Eq. (1)), reaction rates, (−r_{CH4,t}) (Eq. (2)) and sustainability factors, S.F._{CH4} (Eq. (3)) were calculated as follows:

$$X_{CH4,t} = \frac{(F_{in,CH4,t} - F_{out,CH4,t})}{F_{in,CH4,t}} * 100 \quad (1)$$

$$(-r_{CH4,t}) = \frac{X_{CH4,t}}{W/F_{in,CH4,t}} \quad (2)$$

$$S.F._{CH4} = \frac{(-r_{CH4,180min})}{(-r_{CH4,5min})} \quad (3)$$

in Eq. (1), F_{in,CH4,t} and F_{out,CH4,t} represent CH₄ molar flow rates entering (*in*) or leaving (*out*) the reactor at a certain reaction time (*t*). In Eq. (2), W represents the grams of catalyst used, initially loaded in the reactor (oxidized state). In Eq. 3, −r_{CH4,180min} and −r_{CH4,5min} represent CH₄ reaction rates after 180 and 5 min time on stream (TOS), respectively. CH₄ sustainability factor (S.F._{CH4}) was used to compare the stability of the different catalysts over time. If catalyst activity is maintained, the value of the S.F._{CH4} is one. On the other hand, if the catalyst is completely deactivated after 180 min TOS, this value is zero.

Outlet gases composition (syngas composition) was determined by taking bag samples for 2 min and analysing them by means of gas chromatography in a micro GC Varian CP4900 equipped with two packed columns (Molecular Sieve and Porapack) and a TCD detector to quantify H₂, CO, CH₄ and CO₂ concentrations.

2.3. Characterization techniques

The textural properties were measured by N₂ adsorption at 77 K in a Micromeritics Tristar apparatus. The specific surface areas (S_{BET}) and pore volumes (V_p) were calculated by applying the BET method to the respective N₂ adsorption isotherms and the average pore diameter (APD) was calculated with the BJH method based on the adsorption branch of the N₂ isotherm.

XRD patterns of the calcined, reduced and spent catalysts were acquired in a Bruker D8 Advance Series 2 diffractometer equipped with a Cu (λ: 0.154 nm) anode and a secondary graphite monochromator, using a θ-θ configuration. The angle range scanned was 20–80°, using a counting step of 0.05° and a counting time per step of 3 s. The powder XRD patterns were further processed using the accompanying DIFRAC PLUS EVA 8.0 and TOPAS software. For lattice parameter (a) calculations an internal standard (LiB₆) was used to correct the height error.

The reducibility of the calcined catalysts was studied by temperature programmed reduction (TPR) analysis. The respective reduction profiles were obtained in an AutoChem Analyzer II 2920 (Micromeritics) provided with a TCD from a sample amount of 10 mg and using a heat rate of 5 °C min⁻¹ within a temperature range from room temperature to 1050 °C and under a flow rate of 50 mL min⁻¹ of a H₂ (10%)/Ar mixture.

The morphology of the reduced and spent catalysts was studied by transmission electron microscopy (TEM) in a JEOL-2000 FXII microscope operating at 200 keV. Standard TEM copper grids covered by a lacey amorphous carbon film were used as sample holders. The TEM was coupled to an INCA 200-X SIGHT EDX analyser operating between 136 eV and 5.9 keV.

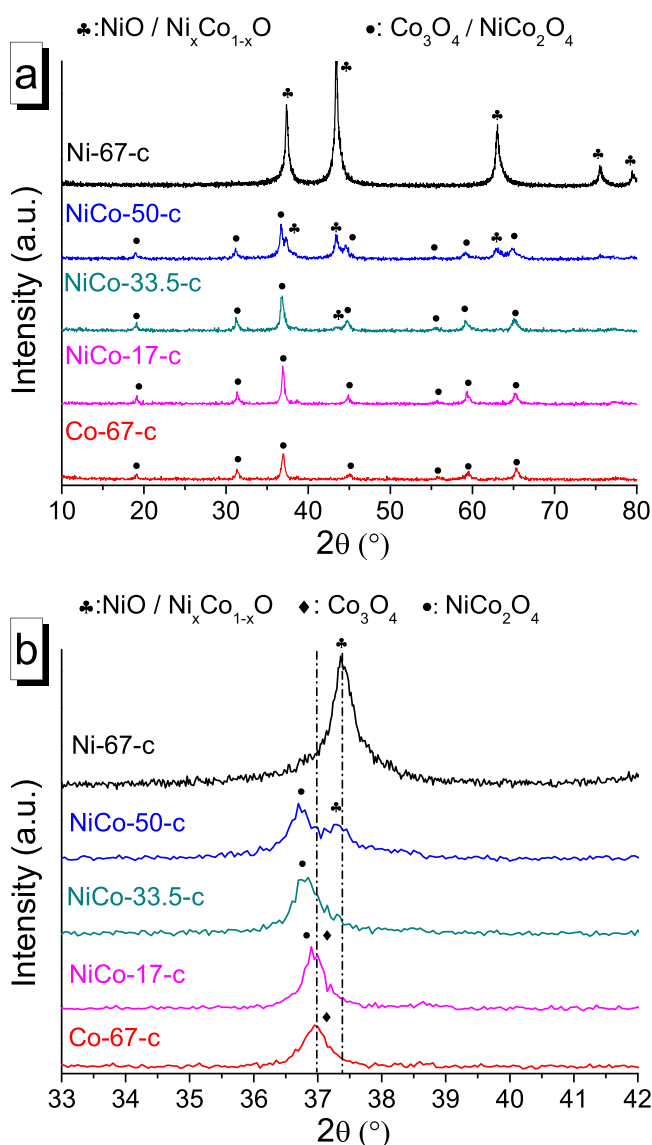


Fig. 1. (a) XRD patterns of the calcined catalysts and (b) magnification of the Co₃O₄ (311) plane and NiO (111) plane.

Carbon production was evaluated by the carbon yield (Y_C) and carbon efficiency (C_E) factors. Y_C , expressed as grams of carbon generated per gram of catalyst ($\text{g}_{\text{carbon}} \text{ g}_{\text{cat}}^{-1}$), was determined in a Setaram Thermogravimetric Analyzer. Samples obtained after reaction were heated under air flow at a rate of $10^\circ\text{C min}^{-1}$ from room temperature to 1000°C . Ni and Co oxidation were taken into account to make calculations. C_E is the ratio between the amount of carbon deposited as calculated from TGA analysis (expressed in mol) and the total amount of methane (mol) converted during the runs (3 h).

3. Results

3.1. Catalysts characterization

The XRD patterns of the calcined NiCo monometallic and bimetallic catalysts are included in Fig. 1a. Ni-67-c and Co-67-c catalysts showed reflections peaks associated to NiO (JCPDS 47-1049) and Co₃O₄ (JCPDS 78-1970), respectively, and presented an average crystal size of 9.1 and 14.5 nm (Table 1). With regard to bimetallic catalysts, NiCo-17-c and NiCo-33.5-c XRD patterns were compara-

Table 1
Textural properties and average crystal domain sizes of the calcined and reduced catalysts.

Catalyst	Textural properties			Crystal size (nm)		
	S _{BET} ($\text{m}^2 \text{ g}^{-1}$)	V _P ($\text{cm}^3 \text{ g}^{-1}$)	APD (nm)	NiO Ni _x Co _{1-x} O	Co ₃ O ₄ NiCo ₂ O ₄	Ni/Co Ni _x Co _{1-x}
Ni-67-c	113	0.145	5.7	9.1	—	—
NiCo-50-c	98	0.127	6.3	8.4	9.0	—
NiCo-33.5-c	73	0.115	7.0	8.1	12.1	—
NiCo-17-c	72	0.075	7.1	—	16.0	—
Co-67-c	57	0.060	3.2	—	14.5	—
Ni-67-r	98	0.162	6.6	—	—	10.9
NiCo-50-r	86	0.133	7.4	—	—	11.3
NiCo-33.5-r	65	0.135	8.1	—	—	11.5
NiCo-17-r	69	0.117	7.8	—	—	12.7
Co-67-r	60	0.090	4.3	—	—	13.8

ble to that of the Co monometallic catalyst, although in the latter a weak diffraction peak around 44° associated to NiO was observed. Finally, the NiCo-50-c XRD pattern presented diffraction peaks that could be ascribed to both NiO and Co₃O₄. Calcined bimetallic catalysts presented average crystal sizes ranging from 8.1 to 16.0 nm, being slightly bigger those associated to Co₃O₄ (Table 1). Due to the simultaneous presence of NiO and Co₃O₄ on the calcined bimetallic catalysts, the formation of mixed oxides is possible although the distinction between NiO/Ni_xCo_{1-x}O and Co₃O₄/NiCo₂O₄ is difficult since their XRD diffraction peaks appear at related angles. However, when the Co₃O₄ diffraction peak related to the plane (311) and located around 37° is magnified (Fig. 1b), a shift to lower angles is observed for both NiCo-33.5-c and NiCo-50-c catalysts with respect to the Co monometallic catalyst. This suggests the formation of NiCo₂O₄ spinel [27]. In this spinel structure, Ni ions occupy octahedral sites and Co ions are distributed among the tetrahedral and octahedral sites [28]. Comparable findings are observed in the NiCo-50-c XRD pattern for the NiO peak located at around 37.5° and related to the plane (111) (Fig. 1b). This can be due to the formation of the Ni_xCo_{1-x}O mixed oxide, as previously reported by other authors [29,30].

XRD patterns of reduced monometallic and bimetallic catalysts are showed in Fig. 2a. In all cases, only diffraction peaks associated to metallic Ni (JCPDS 04-0850) or Co (JCPDS 01-1255) were observed, suggesting a complete reduction of the catalysts. Both metals present a face-centred cubic (fcc) structure which diffraction peaks appear at related angles, thus making difficult to differentiate one from the other. Average crystal domain sizes of reduced catalysts are included in Table 1. An enlargement from 10.9 to 13.8 nm was observed as the Co content of the catalysts increased. In any case, average crystal sizes did not suffer from important changes during the reduction treatment (Table 1). Metallic Ni and Co meet the rules established by Hume-Rothery [31] associated to atomic radius, crystal structures, valence and electronegativity, and therefore it is likely that both metals can form a solid solution. To confirm this point, the lattice constants (a) of each catalyst were measured by means of XRD using an internal standard (LaB₆) to correct height errors. As observed in Fig. 2b, there is a linear relationship between Ni molar fraction of the catalysts and the lattice constant ($R^2 = 0.986$). According to the Vegard's law [32], the compliance of the Hume-Rothery rules along with the linear relationship observed between the lattice constant and the Ni molar fraction, confirms the formation of a Ni_xCo_{1-x} solid solution in the bimetallic reduced catalysts, similarly as reported by other authors [33].

All calcined and reduced catalysts presented a type IV isotherm according to the IUPAC classification which is characteristic of mesoporous materials [34] (Fig. S1 in Supporting information). Bimetallic catalysts presented intermediate S_{BET} and V_P values

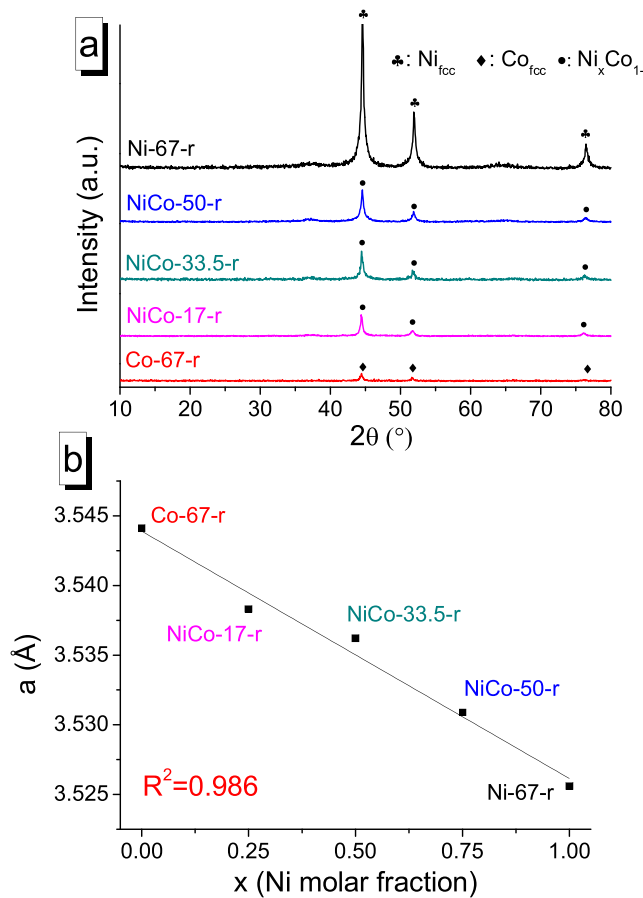


Fig. 2. (a) XRD patterns of the reduced catalysts and (b) lattice constants as a function of the Ni molar fraction in the catalysts.

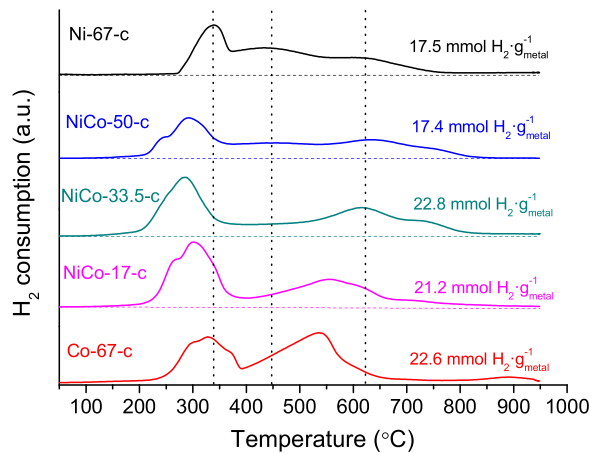


Fig. 3. TPR profiles of the calcined monometallic and bimetallic catalysts.

as compared to monometallic catalysts, as observed in Table 1. Regardless the oxidation state, Ni monometallic catalyst presented the highest S_{BET} and V_p values while Co monometallic catalyst presented the lowest ones. In contrast, the APD of the bimetallic catalysts were larger than those of monometallic catalysts, and the largest APD (8.1 nm) was observed for the NiCo-33.5-r. In addition, a reduction of the S_{BET} was observed after the reduction treatment while an increase of the V_p and APD took place.

TPR profiles of the calcined catalysts are included in Fig. 3. Regarding the Ni-67-c catalyst, three different peaks were observed with maxima at 350, 450 and 610 °C. The TPR profile of this catalyst

was already discussed in [35]. Briefly, the first peak was related to NiO species that do not interact with the Al₂O₃ and it is generally observed when the catalyst active phase content is high, as it occurs with these catalysts (AP:Al molar ratio is 67:33). The second and third peaks were related to NiO species presenting different levels of interaction with the Al₂O₃ and therefore appeared at higher temperatures. Co-67-c catalyst profile presented three reduction regions. The first one was comprised between 200 and 400 °C and it is generally associated to Co₃O₄ species that do not form chemical bonds with the Al₂O₃ [36–38]. Reduction of these species takes place in two steps: Co₃O₄ → 3CoO → 3Co. The peak that appears at medium temperatures (400–650 °C) was related to Co₃O₄ species with some degree of interaction with Al₂O₃. Due to the width of this peak, it is likely that metal and support present different levels of interaction [39,40]. Finally, the small peak observed at high temperatures (850–950 °C) was associated to the presence of CoAl₂O₄ [41,42]. This compound was not detected by XRD since both Co₃O₄ and CoAl₂O₄ present a cubic spinel structure which diffraction peaks appear at the same angles [37]. However, due to the low area of this peak, its formation can be considered minimum. Regarding bimetallic catalysts, a shift of the peak associated to metal species that do not interact with the Al₂O₃ to lower temperatures (300 °C) was observed in all cases. This result suggests a synergistic effect between Ni and Co that favours the reduction of these species. Besides, the shape of the peak resembles the Co monometallic catalyst profile and thus, a reduction process including two or more steps is expected. In contrast, different results were obtained among the bimetallic catalysts profiles when comparing the reduction peaks that are related to metal species that interact with the Al₂O₃. The NiCo-17-c catalyst presented a TPR profile analogous to that of the Co monometallic catalyst, although no peak associated to CoAl₂O₄ reduction was detected. In turn, NiCo-33.5-c and NiCo-50-c presented TPR profiles more alike to that of the Ni monometallic catalyst. Nonetheless, peaks related to NiO species that present different levels of interaction with the Al₂O₃ were shifted to higher temperatures. Total H₂ consumptions expressed per gram of metallic active phase (Ni, Co or Ni + Co) are also included in Fig. 3. The highest H₂ consumption took place during the reduction of the NiCo-33.5-c catalyst (22.8 mmol H₂ g_{metal}⁻¹), although the difference with the Co-67-c consumption was negligible (22.6 mmol H₂ g_{cat}⁻¹). In all cases, total H₂ consumptions calculated by TPR correspond to the theoretical values.

Reduced catalysts were characterized by means of TEM. Regardless the catalyst composition, two different kinds of particles were observed: small metal particles (5–30 nm) inserted into the Al₂O₃ structure and some aggregates of coarse particles. TEM micrographs of Ni-67-r, Co-67-r and NiCo-33.5-r catalysts are included in the Supporting information (Fig. S2).

3.2. Catalysts activity and stability in the CDB

In order to test the performance of the NiCo bimetallic catalysts, experiments were carried out at 700 °C, 120 L_N g_{cat}⁻¹ h⁻¹ and a CH₄:CO₂ ratio of 60:40. Results obtained with monometallic catalysts are included for comparison reasons. Catalysts performance was evaluated considering their activity at the beginning of the experiments (5 min TOS), stability (180 min TOS), carbon yield (Y_C) and carbon efficiency (C_E). Values of the most representative parameters used are included in Table 2.

CH₄ conversion after 5 min TOS followed this order: NiCo-50-r > Ni-67-r ~ NiCo-33.5-r > NiCo-17-r > Co-67-r. Regarding CO₂ conversion, some differences were observed as compared with CH₄ conversion results. Bimetallic catalysts presented higher CO₂ conversions than monometallic catalysts. In addition, it was noteworthy that the difference between the CO₂ conversions obtained

Table 2

CH_4 and CO_2 conversions, syngas H_2 and CO concentrations (v:v, dry basis) and $\text{H}_2:\text{CO}$ ratio obtained after 5 min TOS and CH_4 sustainability factor, carbon yield and carbon efficiency obtained after 180 min TOS at 700°C and $120 \text{ L}_N \text{ g}_{\text{cat}}^{-1} \cdot \text{h}^{-1}$.

Catalyst	X_{CH_4} (%)	X_{CO_2} (%)	H_2 (%)	CO (%)	ratio $\text{H}_2:\text{CO}$	S.F. $_{\text{CH}_4}$ (-)	Y_C ($\text{g}_C \text{ g}_{\text{cat}}^{-1}$)	C_E ($\text{mol}_C \cdot \text{mol}_{\text{CH}_4}^{-1} \times 100$)
Ni-67-r	64.0	76.2	42.9	37.2	1.15	0.57	7.4	14.1
NiCo-50-r	66.7	83.7	45.7	38.4	1.19	0.51	7.7	15.9
NiCo-33.5-r	63.0	80.0	43.7	37.5	1.17	0.69	12.1	21.7
NiCo-17-r	56.6	78.7	40.2	38.0	1.06	0.61	6.9	15.6
Co-67-r	47.2	69.2	35.0	34.5	1.01	0.64	2.0	5.7

with the Ni and Co monometallic catalysts (7%) was considerably lower than the difference between CH_4 conversions values (16.8%).

Considering H_2 and CO concentrations of the syngas produced, a similar trend to that observed with CH_4 and CO_2 conversions was observed. Highest H_2 concentrations were obtained with the catalysts with a high Ni content (Ni-67-r, NiCo-50-r and NiCo-33.5-r) and CO concentrations obtained with the bimetallic catalysts were higher than those obtained with the monometallic catalysts. As regard to the $\text{H}_2:\text{CO}$ ratio, syngas obtained with the NiCo-50-r and NiCo-33.5-r catalysts presented the highest values, 1.19 and 1.17 respectively. On the other hand, the lowest $\text{H}_2:\text{CO}$ ratio was obtained with the Co monometallic catalyst followed by the NiCo-17-r catalyst. Carbon formation in DCB can be associated to CH_4 decomposition ($\text{CH}_4 \rightarrow 2\text{H}_2 + \text{C}$) and carbon gasification to CO formation ($\text{CO}_2 + \text{C} \rightarrow 2\text{CO}$) and thus, carbon formation potential can be related to the $\text{H}_2:\text{CO}$ ratio. Therefore, Ni-67-r, NiCo-50-r and NiCo-33.5-r catalysts presented at the beginning of the experiment higher carbon formation potential than NiCo-17-r and Co-67-r catalysts.

Regarding catalyst stability, S.F. $_{\text{CH}_4}$ values are included in Table 2. Due to the fact that S.F. $_{\text{CH}_4}$ values are lower than one, it can be concluded that all catalysts suffered, under these reaction conditions, from some degree of deactivation during the experiments. The stability of the catalysts is also reflected on the evolution of $-r_{\text{CH}_4}$ over time (Fig. 4a). A progressive decrease of $-r_{\text{CH}_4}$ with time was observed in all the experiments. However, different deactivation behaviours were detected. Ni-67-r and NiCo-33.5-r catalysts presented analogous $-r_{\text{CH}_4}$ curves during the first 60 min TOS. Then, Ni-67-r deactivation was more pronounced and as a result lower $-r_{\text{CH}_4}$ values were obtained as compared with those of the NiCo-33.5-r. On the other hand, Co-67-r and NiCo-17-r catalysts suffered an important decrease of $-r_{\text{CH}_4}$ during the first 30 min TOS. Afterwards, Co-67-r catalyst reached a steady state while the activity of the NiCo-17-r catalyst continued decreasing although the rate of deactivation was lower. Finally, $-r_{\text{CH}_4}$ evolution of the NiCo-50-r presented an intermediate behaviour since a constant drop of $-r_{\text{CH}_4}$ took place along the whole experiment: at the beginning of the experiment (5 min TOS), $-r_{\text{CH}_4}$ was slightly higher than those obtained with the Ni-67-r and NiCo-33.5-r catalysts while after 180 min TOS the situation was reversed and its value was close to the NiCo-17-r one. As a result, this catalyst presented the lowest S.F. $_{\text{CH}_4}$ value.

The evolution of the $\text{H}_2:\text{CO}$ ratio over time is showed in Fig. 4b. Comparable trends to those commented for $-r_{\text{CH}_4}$ were observed. It was noteworthy that the $\text{H}_2:\text{CO}$ ratio obtained with the Co-67-r catalyst was lower than one after only 15 min TOS and afterwards its value stabilized around 0.8. In contrast, the $\text{H}_2:\text{CO}$ ratio obtained with high Ni content catalysts (Ni-67-r, NiCo-50-r and NiCo-33.5-r) remained over one during at least 60 min TOS.

Carbon yields obtained with the monometallic and bimetallic catalysts are included in Table 2. As observed, the highest yield was obtained with the NiCo-33.5-r catalyst. Carbon produced, $12.1 \text{ g}_C \text{ g}_{\text{cat}}^{-1}$, was considerably higher than the one obtained with the Ni monometallic catalyst. In turn, NiCo-50-r and NiCo-17-r produced comparable carbon yields as Ni-67-r. Especially remarkable

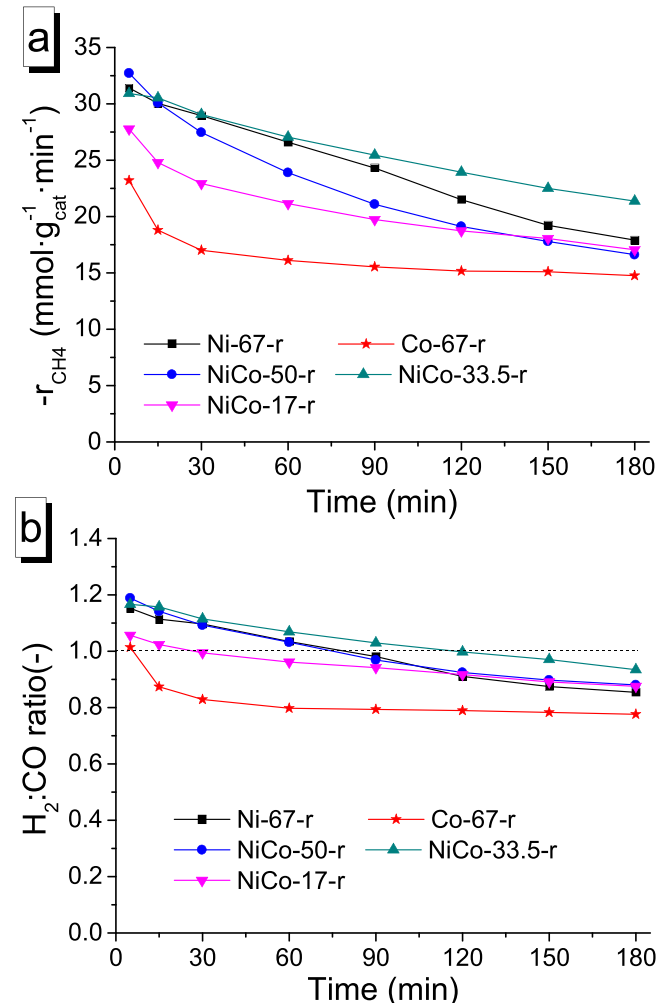


Fig. 4. (a) CH_4 reaction rate ($-r_{\text{CH}_4}$) and (b) $\text{H}_2:\text{CO}$ ratio as a function of TOS for the different catalysts at 700°C and $120 \text{ L}_N \text{ g}_{\text{cat}}^{-1} \cdot \text{h}^{-1}$.

was the carbon formed with the NiCo-17-r catalyst. Despite the fact that its catalyst composition was close to the Co-67-r catalyst, its Y_C was more than 3 times higher, $6.9 \text{ g}_C \text{ g}_{\text{cat}}^{-1}$ vs. $2.0 \text{ g}_C \text{ g}_{\text{cat}}^{-1}$. Carbon efficiency followed the same trend as the Y_C , although the highest value obtained for the NiCo-33.5-r ($21.7 \text{ mol}_C \text{ mol}_{\text{cat}}^{-1}$) was relatively low, which indicates the poor efficiency of the process in terms of carbon formation, mainly due to the relatively high WHSV used.

Given that the main objective of the CDB process is the production of carbon nanomaterials and according to the results previously commented, additional experiments were carried out with the NiCo-33.5-r catalyst at 600 and 700°C and $30 \text{ L}_N \text{ g}_{\text{cat}}^{-1} \cdot \text{h}^{-1}$. For comparison reasons, experiments at the same conditions were carried out with the monometallic catalysts. Fig. 5 shows $-r_{\text{CH}_4}$ evolution over time for the three catalysts. At 600°C (solid lines), initial

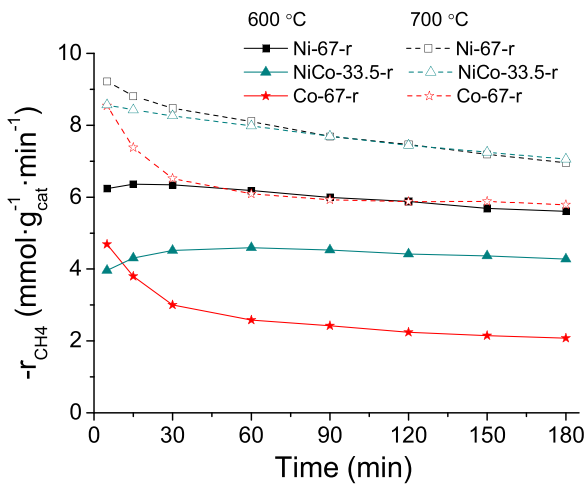


Fig. 5. CH₄ reaction rate for the different catalysts at 30 L_N g_{cat}⁻¹ h⁻¹ and 600 (solid lines) and 700 °C (dash lines).

Table 3

CH₄ sustainability factor carbon yield and carbon efficiency obtained after 180 min TOS at 600 and 700 °C and 30 L_N g_{cat}⁻¹·h⁻¹.

Temp.	Catalyst	S.F. _{CH₄} (-)	Y _C (g _C ·g _{cat} ⁻¹)	C _E (mol _C ·mol _{CH₄CH₄} ⁻¹ × 100)
600 °C	Ni-67-r	0.90	8.8	67.8
	NiCo-33.5-r	1.08	5.8	60.7
	Co-67-r	0.44	1.1	19.2
700 °C	Ni-67-r	0.75	6.8	40.15
	NiCo-33.5-r	0.82	6.6	39.4
	Co-67-r	0.68	3.7	22.4

catalyst activity of the NiCo-33.5-r was comparable to that of the Co-67-r and significantly lower than that of the Ni-67-r catalyst. In contrast, when temperature was increased up to 700 °C (dash lines), initial $-r_{\text{CH}_4}$ presented almost the same values. As respect to catalyst stability, i.e. the evolution of $-r_{\text{CH}_4}$ over time, comparable results as those observed in Fig. 4 were found. Regardless the reaction temperature, the $-r_{\text{CH}_4}$ evolution over time obtained with the NiCo-33.5-r and Ni-67-r catalysts were very similar. At 600 °C, both catalysts suffered a little induction period at the early stage of the experiment during which $-r_{\text{CH}_4}$ increased and after reaching a maximum, it decreased slowly. Analogous results were observed at 700 °C although no induction period took place. In contrast, $-r_{\text{CH}_4}$ values obtained with the Co-67-r decreased quickly during the first 30–60 min TOS at both 600 and 700 °C and thereafter a steady state was reached. This induction period can be tentatively explained by a reorganization and fractioning of the catalyst particle at the early stages of the reaction, resulting in the formation of the active crystallites that promote the CNF formation. This induction period is only observed at relatively slower reaction rates, i.e tests carried out at 600 °C and 30 L_N g_{cat}⁻¹ h⁻¹. However, it is likely that this induction period also takes place at higher space velocities/higher temperatures, although it is not observed due to the speed of the process triggered by the higher reaction rates.

S.F._{CH₄} values are included in Table 3. Regardless the reaction temperature, NiCo-33.5-r presented higher S.F._{CH₄} values than monometallic catalysts and therefore it appeared as the most stable catalyst. It was noteworthy that at 600 °C, the S.F._{CH₄} value obtained was higher than one (1.08). This value means that this catalyst was more active at the end than at the beginning of the experiment. This situation was the result of two combined effects: the induction period previously commented and the great stability of the catalyst at these experimental conditions. In contrast, the S.F._{CH₄} obtained with the Co-67-r catalyst at 600 °C was significantly low.

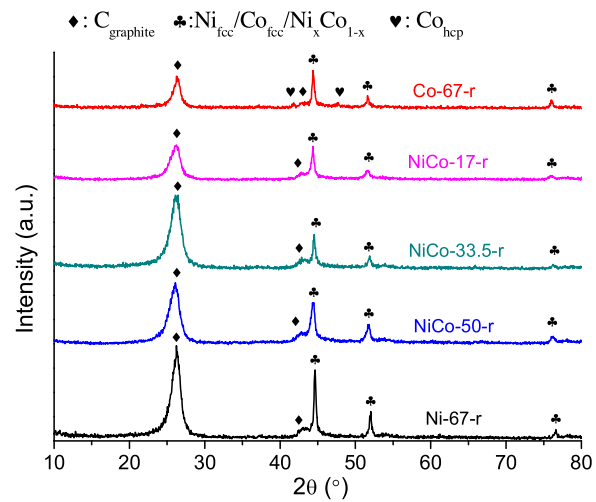


Fig. 6. XRD patterns of the carbonaceous materials obtained after the reaction.

By increasing reaction temperature from 600 to 700 °C, a decrease of stability was observed for both Ni-67-r and NiCo-33.5-r while an increase took place for the Co-67-r catalyst. In any case, the value obtained (0.68) was still lower than those obtained with the Ni containing catalysts.

Y_C and C_E also varied depending on reaction temperature and catalyst (Table 3). At both temperatures, the highest values were obtained with the Ni-67-r catalyst. However, the differences with the NiCo-33.5-r catalyst were negligible at 700 °C. In turn, C_E and Y_C obtained with the Co monometallic catalyst were much lower, especially at 600 °C. The importance of the reaction conditions can be assessed by the C_E factor. Thus, lower temperatures and WHSV favour carbon formation, and the highest C_E value was obtained for the Ni-67-r catalyst at 600 °C and 30 L_N g_{cat}⁻¹ h⁻¹ (67.8), although overall a good compromise between S.F._{CH₄} and both Y_C and C_E was obtained with the NiCo-33.5-r.

3.3. Carbon nanofilaments characterization

Carbonaceous materials (carbon + spent catalyst) obtained with bimetallic and monometallic catalysts at 700 °C and 120 L_N g_{cat}⁻¹ h⁻¹ were characterized by XRD, N₂ adsorption and TEM. XRD patterns of the carbonaceous materials are showed in Fig. 6. All samples presented an intense peak around 26° due to graphitic carbon formation. It was noticeable the absence of peaks associated to Ni or Co oxidized species (NiO, Co₃O₄, CoO) and therefore it is likely that metals remained in their reduced phase during reaction. No differences were inferred between bimetallic and Ni monometallic catalysts XRD patterns. However, considering the sample produced with the Co-67-r catalyst, the presence of small peaks around 41.8° and 47.7° suggest the formation of hexagonal close-pack Co (hcp-Co) as previously discussed in [43].

Carbon structural parameters are included in Table 4. As it is observed, carbon materials obtained with the bimetallic catalysts presented slightly higher d₀₀₂ values than monometallic catalysts and lower L_C values. These results suggest that bimetallic catalysts lead to the formation of less graphitic carbon materials. Regarding Ni/Co crystal sizes, all samples presented a higher value as compared to reduced catalysts (Table 1). Nevertheless, the increase was more pronounced in monometallic catalysts.

Textural properties of the carbonaceous samples are also included in Table 4. Carbon yields obtained with bimetallic catalysts were high enough to consider that textural properties of the samples came from carbon nanofilaments rather than from catalyst particles. Samples obtained with the bimetallic catalysts presented

Table 4

Specific surface, pore volume, average pore diameter, interplanar distance, carbon crystal domain size, Ni/Co crystal domain size and carbon nanofibres diameter of the carbonaceous materials obtained after reaction.

Material	Textural properties			XRD			TEM
	S_{BET} $\text{m}^2 \text{ g}^{-1}$	V_p $\text{cm}^3 \text{ g}^{-1}$	APD nm	d_{002} nm	L_c nm	$d_{\text{Ni/Co}}$ nm	
Ni-67-r	95	0.431	22.0	0.338	6.2	28.4	19.9 ± 11.3
NiCo-50-r	116	0.524	13.5	0.341	5.3	14.2	n.a.
NiCo-33.5-r	123	0.580	13.8	0.340	5.3	22.6	21.4 ± 6.0
NiCo-17-r	110	0.462	13.0	0.339	5.7	18.0	n.a.
Co-67-r	73	0.242	11.2	0.337	8.2	25.8	20.9 ± 8.2

comparable textural properties. Nonetheless, the highest S_{BET} , V_p and APD values were those of the carbonaceous sample produced with the NiCo-33.5-r catalyst.

Carbonaceous material produced at 700°C and $120 \text{ L}_N \text{ g}_{\text{cat}}^{-1} \text{ h}^{-1}$ with the NiCo-33.5-r catalyst was selected to be further characterized by TEM. Samples obtained with monometallic catalysts were also characterized for comparison reasons. Representative TEM micrographs are showed in Figs. 7 and 8. Low magnification micrographs of the samples (Fig. 7) revealed the presence of two types of carbon: encapsulating carbon and nanofilamentous carbon. These types of carbon were observed in all samples, although their concentration varied. While samples produced with the Ni-67-r and NiCo-33.5-r catalysts were mainly composed by carbon nanofilaments, the sample produced with the Co monometallic catalyst presented a larger proportion of carbon encapsulating big Co particles. This trend was also observed for the carbonaceous samples obtained at different reaction conditions (600°C , $30 \text{ L}_N \text{ g}_{\text{cat}}^{-1} \text{ h}^{-1}$; 700°C , $30 \text{ L}_N \text{ g}_{\text{cat}}^{-1} \text{ h}^{-1}$, figures not shown).

The different type of carbons observed by TEM (encapsulating carbon and carbon nanofibers), can also be assessed by using thermogravimetric analysis. This differentiation can be done thanks to the different resistance to oxidation shown by the two types of carbons present in the samples, resulting in differences in the DTG curves (Fig. S4). Thus, DTG curves of carbonaceous sample produced with the Co-67-r catalyst displayed two well defined peaks: a large peak appearing at relatively lower temperatures ascribed to CNF and a small peak at higher oxidation temperature associated to encapsulating carbon with a more graphitic nature. This second peak is absent in the samples obtained with Ni-67-r and NiCo-33.5-r catalysts, thus supporting TEM observation, i.e., Co-67 catalyst had a larger amount of encapsulating carbon as reflected by the peak appearing at relative higher temperatures.

High magnification micrographs are showed in Fig. 8. Two different carbon nanofilaments structures were observed in the sample obtained with the Ni monometallic catalyst: fishbone (Fig. 8a) and parallel (Fig. 8b) carbon nanofibres. However, it is likely that a carbon nanofibre of this sample can contain both structures along its length because as reported in [43], the inclination of the graphene layers depend on the angle α formed by the walls of the particle at its trailing face and the shape of the particle vary throughout the reaction. As observed in Fig. 8a, at the beginning of the reaction, graphene layers adopted a fishbone configuration. However, as the reaction took place, the catalyst particle was elongated and as a result, graphene layers turned into a parallel configuration. In contrast, carbon nanofilaments produced with the Co-67-r catalyst only presented a parallel structure (Fig. 8c). It is likely that carbon nanofibre formation over the Co-67-r catalyst followed a different mechanism as compared with the Ni-67-r catalyst. This hypothesis is supported by Fig. 8d, where the first graphene layers of a carbon nanofibre formed from a Co particle are showed. As it is observed, graphene layers adopted a parallel configuration at the early stage of the reaction. Finally, Fig. 8e and f reveal the formation of both fishbone and parallel like carbon nanofibres with the NiCo-33.5-r

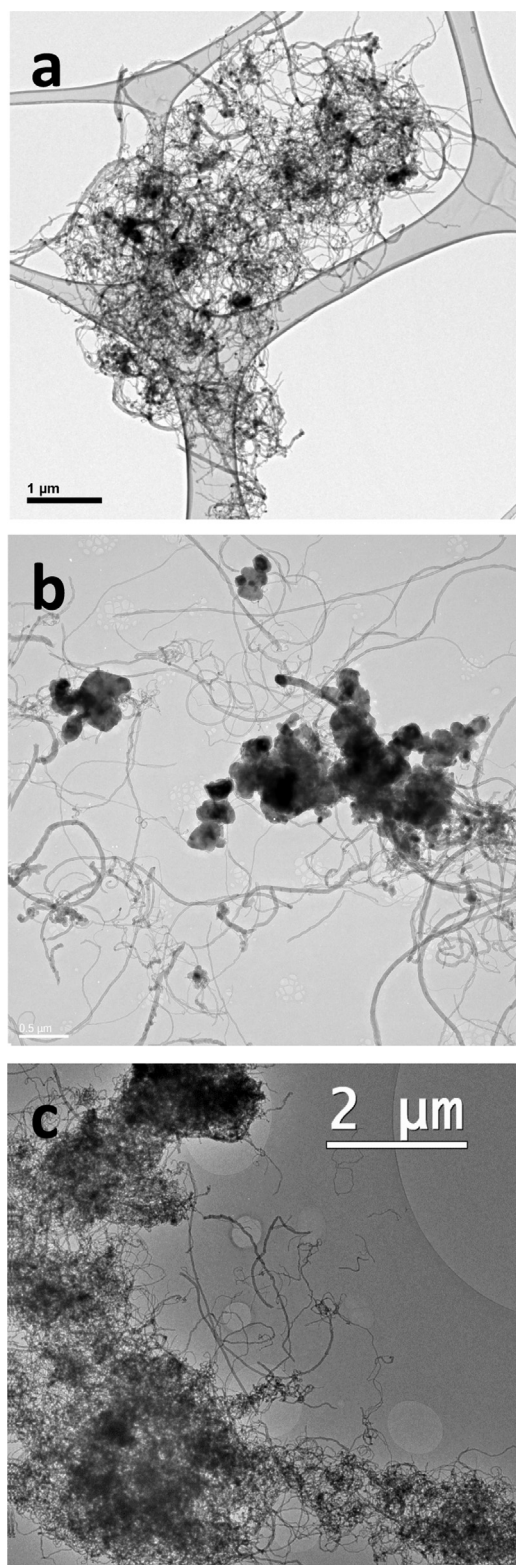


Fig. 7. Low magnification TEM micrographs of the carbonaceous samples produced at 700°C and $120 \text{ L}_N \text{ g}_{\text{cat}}^{-1} \text{ h}^{-1}$ with (a) Ni-67-r, (b) Co-67-r and (c) NiCo-33.5-r catalysts.

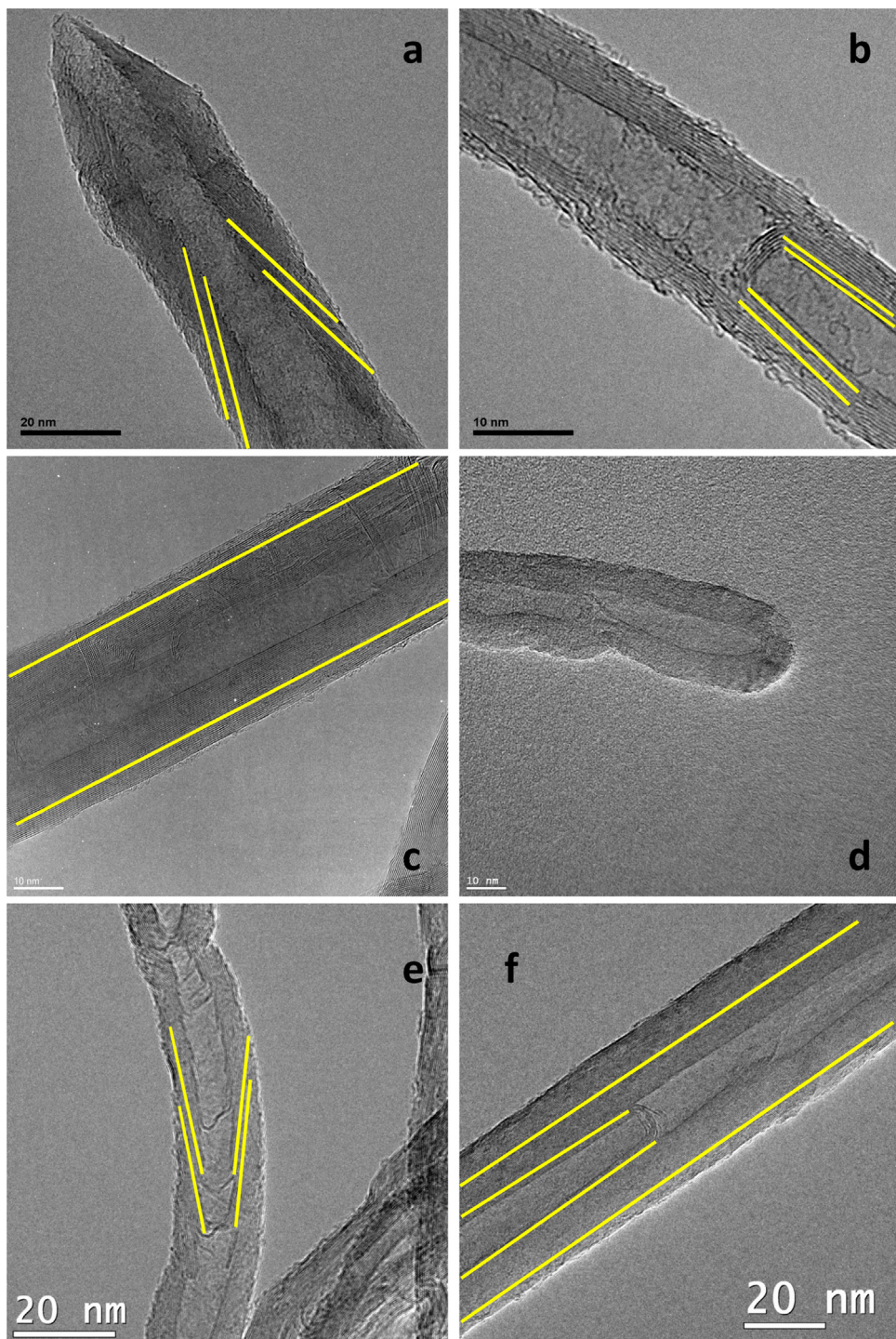


Fig. 8. TEM micrographs of the carbonaceous samples produced at 700 °C and $120 \text{ L}_N \text{ g}_{\text{cat}}^{-1} \text{ h}^{-1}$ with (a) and (b) Ni-67-r, (c) and (d) Co-67-r and (e) and (f) NiCo-33.5-r catalysts.

catalyst. These structures are the same as those obtained with the Ni monometallic catalyst.

4. Discussion

In general, bimetallic catalysts showed a good performance during the CDB. Especially relevant was the carbon yield obtained with the NiCo-17-r catalyst at 700 °C and $120 \text{ L}_N \text{ g}_{\text{cat}}^{-1} \text{ h}^{-1}$. In spite of its catalyst composition, more alike to the Co-67-r catalyst than to the Ni-67-r catalyst, the carbon formed was considerably higher

than that produced with the Co-67-r catalyst, 6.9 and $2.0 \text{ g}_C \text{ g}_{\text{cat}}^{-1}$, respectively (Table 2). Moreover, due to the fact that carbon yields obtained with the bimetallic catalysts were close or even higher than that achieved with the Ni-67-r catalyst (Table 2), it is likely that these catalysts behave similarly as far as carbon formation is concerned. This result suggests that the incorporation of a small percentage of Ni modifies the mechanisms involved in carbon nanofilaments formation [44], which comprises of different stages: (i) CH_4 decomposition in the active sites of metal particles to form reactive carbon, (ii) carbon diffusion over the catalyst particles sur-

face and/or through the catalyst bulk and (iii) carbon nucleation in the trailing face of the catalyst particles to the formation of carbon nanofilaments. In particular, the kind of carbon nanofilament structures observed in the TEM micrographs suggests that the carbon diffusion (stage ii) changed upon the addition of small amounts of Ni (Fig. 8). As previously commented, only parallel carbon nanofilaments were formed with the Co-67-r catalyst and according to shape of the carbon nanofilament tip showed in Fig. 8d, it may occur that carbon only diffuses over the surface of the Co particles from the front face to the trailing face as proposed by Baird et al. [45] or Oberlin et al. [46] for Fe based catalysts. In contrast, a mixture of parallel and fishbone structures were observed in the samples produced with the Ni-67-r and NiCo-33.5-r catalysts. According to the shape of the carbon nanofilament tip observed in Fig. 7a and due to the fact that solid carbon nanofibres were obtained with these catalysts at 600 °C (Fig. S3), it is likely that carbon diffuses simultaneously over the catalyst particle surface and through the catalyst bulk during carbon nanofilament formation when using the Ni-67-r or the bimetallic catalysts.

The distinct evolutions of $-r_{CH_4}$ over time showed in Fig. 4 reveal differences between catalysts that can also be related to different carbon formation/removal mechanisms. Co-67-r catalyst suffered an important deactivation during the first 30 min TOS and afterwards it reached a steady state (Fig. 4a). Even though an increase of the average Co crystal size from 13.8 to 25.8 nm took place during reaction, it is more likely that the activity loss observed was related to a rapid formation of encapsulating carbon since crystal size enlargement was also observed for the Ni-67-r catalyst (Tables 2 and 4). Besides this, analogous CNF average diameters, which are related to the Ni/Co crystal domain size, were obtained for all catalyst tested. This allows us to establish that the main benefit from NiCo bimetallic catalyst is the better carbon diffusion, ruling out the effect of the crystal domain size.

It is well known that encapsulating carbon is formed as a result of an imbalance between carbon formation rate and carbon removal rate on the surface of the catalyst particles and simplifying, in the CDB the former is related to CH₄ decomposition rate (CH₄ → 2H₂ + C) and the latter to a combination of carbon gasification by CO₂ (CO₂ + C → 2CO) and carbon diffusion to generate a carbon nanofilament. In spite of showing a low carbon formation potential (low ratio H₂:CO) and a high CO₂ conversion, the Co-67-r catalyst was rapidly deactivated. Therefore, results suggest that Co monometallic catalyst presented a lower ability for surface carbon diffusion from the front face to the trailing face to generate a carbon nanofilament and as a result, encapsulating carbon was formed. Carbon yields obtained in this work agree with those reported by Xu et al. [23] who studied different NiCo bimetallic catalysts in the DRM. They observed that bimetallic catalysts presented higher cooking rates than a Co monometallic catalyst and that the bimetallic catalyst with an equimolar Ni/Co composition led to the highest carbon deposition.

In addition to the aforementioned different carbon nanofilament formation mechanisms and ability to remove surface carbon by diffusion, the low carbon yield obtained with the Co monometallic catalyst can also be related to the formation of hcp-Co as previously discussed in [43]. hcp-Co is unstable above 450 °C [47] and its presence above this temperature has been related to the formation of graphitic carbon encapsulating Co particles [48]. While hcp-Co was observed in the XRD pattern of the carbonaceous sample obtained with the Co-67-r catalyst, it was not detected in the XRD patterns of the samples produced with the bimetallic catalysts (Fig. 6). In any case, the intensity of the hcp-Co peaks was low.

As previously commented, one of the main objectives of the CDB process is the production of carbon nanofilaments. Therefore, the most important result obtained along this work was the high Y_C obtained with the NiCo-33.5-r catalyst at 700 °C and

120 L_N g_{cat}⁻¹ h⁻¹ (12.1 g_C g_{cat}⁻¹). The activity (-r_{CH₄} values) and stability (S.F._{CH₄}) of the NiCo-33.5-r catalyst were identical to those obtained with the Ni-67-r catalyst during the first 60 min TOS (Fig. 4a). However, the NiCo-33.5-r bimetallic catalyst showed a better performance (higher -r_{CH₄}) afterwards that resulted in a greater carbon formation. Besides, it was observed in Fig. 4b that the bimetallic catalyst presented higher H₂:CO ratio values throughout the entire experiment than the other catalysts and therefore a higher carbon formation potential. Probably, the good stability showed by the NiCo-33.5-r catalyst at these reaction conditions was related to a synergistic effect between Ni and Co. Carbon yields obtained (Table 2) and the kind of carbon structures formed (Fig. 8) suggest that Ni monometallic and bimetallic catalysts presented comparable behaviours as far as carbon formation is concerned and therefore, the presence of Ni favoured surface carbon diffusion as compared to Co monometallic catalyst. In turn, the presence of Co favoured soot and carbon particles oxidation via redox reactions as previously reported [49–51] and as a result, the accumulation of carbon on the surface of the catalyst particles is reduced. The combination of both effects allows that the NiCo-33.5-r catalyst was able to produce an important amount of carbon nanofilaments maintaining a good catalyst stability.

Nevertheless, when the space velocity was decreased from 120 to 30 L_N g_{cat}⁻¹ h⁻¹, the good performance of the NiCo-33.5-r catalyst related to carbon formation was not maintained. At 600 °C, the low carbon yield obtained with the bimetallic catalyst as compared to the Ni monometallic catalyst was due to its lower -r_{CH₄} (Fig. 5). In turn, at 700 °C, both catalysts presented analogous -r_{CH₄} and almost identical deactivation curves (Fig. 5) and therefore, carbon yields obtained were very close (Table 4). As observed in Fig. 5, the maximum -r_{CH₄} achieved with the NiCo-33.5-r catalyst coincided with those of the Co-67-r catalyst at both 600 and 700 °C suggesting that the activity of bimetallic catalysts is limited by the activity of Co. For that reason, the carbon yield obtained with the NiCo-33.5-r at 600 °C was lower than that obtained with the Ni monometallic catalyst. It has to be noted that the lower activity showed by the Co-67-r catalyst as compared to bimetallic catalysts in Fig. 4 was probably related to its rapid deactivation due to the fact that a high space velocity was used (120 L_N g_{cat}⁻¹ h⁻¹). On the other hand, by reducing the space velocity, differences related to catalyst stability cannot be observed during the 180 min of reaction as it occurred at 700 °C and 120 L_N g_{cat}⁻¹ h⁻¹, provoking that almost same carbon yields were obtained at 700 °C and 30 L_N g_{cat}⁻¹ h⁻¹. However, if we attend to the carbon efficiency, it is clear that lower temperatures and WHSV favour carbon formation.

5. Conclusions

NiCo bimetallic catalysts appear as an interesting alternative to Ni monometallic catalyst for the production of carbon nanofilaments using biogas as carbon feedstock. Bimetallic catalyst with an equimolar Ni/Co composition showed the highest carbon yield and sustainability factor at 700 °C and 120 L_N g_{cat}⁻¹ h⁻¹. Its good performance was related to a synergistic effect between Ni and Co: the presence of Ni favoured surface carbon diffusion while the presence of Co favoured soot and carbon particles oxidation via redox. The combination of both effects allows that the NiCo-33.5-r catalyst was able to produce an important amount of carbon nanofilaments maintaining good catalyst stability. However, the better performance of this catalyst as compared to the Ni-67-r catalyst was not maintained when reducing the space velocity from 120 to 30 L_N g_{cat}⁻¹ h⁻¹ and temperature from 700 to 600 °C because bimetallic catalyst activity was linked to Co monometallic activity that at 600 °C was considerably lower than that of the Ni monometallic catalyst.

Acknowledgments

This work was funded by FEDER and the Spanish Economy and Competitiveness Ministry (MINECO) (ENE2011-28318-C03-01 and ENE2014-52189-C02-01-R). JLP thanks MINECO for his Ramon y Cajal research contract (RYC-2013-12494). S. de Llobet thanks the Diputación General de Aragón for the Ph.D. grant.

Appendix A. Supplementary data

Supplementary data associated with this article can be found, in the online version, at <http://dx.doi.org/10.1016/j.apcatb.2016.07.015>.

References

- [1] J.L. Walsh, C.C. Ross, M.S. Smith, S.R. Harper, *Biomass* 20 (1989) 277–290.
- [2] W. Keim, *Pure Appl. Chem.* 58 (1986) 825–832.
- [3] Y.H. Hu, E. Ruckenstein, *Adv. Catal.* 48 (2004) 297–345.
- [4] M.C.J. Bradford, M.A. Vannice, *Catal. Rev. Sci. Eng.* 41 (1999) 1–42.
- [5] J.R. Rostrup-Nielsen, J.H.B. Hansen, *J. Catal.* 144 (1993) 38–49.
- [6] J.L. Pinilla, S. de Llobet, I. Suelves, R. Utrilla, M.J. Lázaro, R. Moliner, *Fuel* 90 (2011) 2245–2253.
- [7] C.H. Bartholomew, *Catal. Rev.* 24 (1982) 67–112.
- [8] Z.L. Zhang, X.E. Verykios, *Catal. Today* 21 (1994) 589–595.
- [9] D.L. Trimm, *Catal. Today* 37 (1997) 233–238.
- [10] V.C.H. Kroll, H.M. Swaan, C. Mirodatos, *J. Catal.* 161 (1996) 409–422.
- [11] P.G. Menon, *J. Mol. Catal.* 59 (1990) 207–220.
- [12] J.L. Pinilla, R. Moliner, I. Suelves, M.J. Lázaro, Y. Echegoyen, J.M. Palacios, *Int. J. Hydrol. Energy* 32 (2007) 4821–4829.
- [13] N.M. Rodriguez, *J. Mater. Res.* 8 (1993) 3233–3250.
- [14] J. Zhu, A. Holmen, D. Chen, *ChemCatChem* 5 (2013) 378–401.
- [15] P. Serp, M. Corriás, P. Kalck, *Appl. Catal. A* 253 (2003) 337–358.
- [16] L. Dai, D.W. Chang, J.B. Baek, W. Lu, *Small* 8 (2012) 1130–1166.
- [17] E. Hammel, X. Tang, M. Trampert, T. Schmitt, K. Mauthner, A. Eder, P. Pötschke, *Carbon* 42 (2004) 1153–1158.
- [18] S. de Llobet, J.L. Pinilla, M.J. Lázaro, R. Moliner, I. Suelves, *Int. J. Hydrol. Energy* 37 (2012) 7067–7076.
- [19] S. De Llobet, J.L. Pinilla, M.J. Lazaro, R. Moliner, I. Suelves, *Fuel* 111 (2013) 778–783.
- [20] S. De Llobet, J.L. Pinilla, R. Moliner, I. Suelves, *Fuel* 139 (2014) 71–78.
- [21] J. Zhang, H. Wang, A.K. Dalai, *J. Catal.* 249 (2007) 300–310.
- [22] J. Zhang, H. Wang, A.K. Dalai, *Appl. Catal. A* 339 (2008) 121–129.
- [23] J. Xu, W. Zhou, Z. Li, J. Wang, J. Ma, *Int. J. Hydrol. Energy* 34 (2009) 6646–6654.
- [24] K. Takanabe, K. Nagaoaka, K. Nariai, K. Aika, *J. Catal.* 232 (2005) 268–275.
- [25] L. Chen, Q. Zhu, R. Wu, *Int. J. Hydrol. Energy* 36 (2011) 2128–2136.
- [26] I. Suelves, M.J. Lázaro, R. Moliner, Y. Echegoyen, J.M. Palacios, *Catal. Today* 116 (2006) 271–280.
- [27] V.M. Gonzalez-delaCruz, R. Pereñiguez, F. Ternero, J.P. Holgado, A. Caballero, *J. Phys. Chem. C* 116 (2011) 2919–2926.
- [28] O. Knop, K.I.G. Reid, Sutarno, Y. Nakagawa, *Can. J. Chem.* 46 (1968) 3463–3476.
- [29] A.P.S. Peres, A.C. Lima, B.S. Barros, D.M.A. Melo, *Mater. Lett.* 89 (2012) 36–39.
- [30] T. Mandzhukova, J.-L. Bobet, M. Khrussanova, P. Peshev, *Mater. Res. Bull.* 44 (2009) 1968–1972.
- [31] W. Hume-Rothery, B.R. Coles, *Atomic Theory for Students of Metallurgy*, Institute of Metals, London: Brookfield, VT, USA, 1988.
- [32] A.R. Denton, N.W. Ashcroft, *Phys. Rev. A* 43 (1991) 3161–3164.
- [33] K. Takanabe, K. Nagaoaka, K. Nariai, K.I. Aika, *J. Catal.* 232 (2005) 268–275.
- [34] K.S.W. Sing, D.H. Everett, R.A.W. Haul, L. Moscou, R.A. Pierotti, J. Rouquérol, T. Siemieniewska, *Pure Appl. Chem.* 57 (1985) 603–619.
- [35] S. de Llobet, J.L. Pinilla, R. Moliner, I. Suelves, *Appl. Catal. B* 165 (2015) 457–465.
- [36] R. Brown, M.E. Cooper, D.A. Whan, *Appl. Catal. A* 3 (1982) 177–186.
- [37] B. Jongsomjit, J. Panpranon, J.G. Goodwin Jr., *J. Catal.* 204 (2001) 98–109.
- [38] Y. Zhang, H. Xiong, K. Liew, J. Li, *J. Mol. Catal. A: Chem.* 237 (2005) 172–181.
- [39] P. Arnoldy, J.A. Moulijn, *J. Catal.* 93 (1985) 38–54.
- [40] G. Jacobs, T.K. Das, P.M. Patterson, J. Li, L. Sanchez, B.H. Davis, *Appl. Catal. A* 247 (2003) 335–343.
- [41] A. Lapidus, A. Krylova, V. Kazanskii, V. Borovkov, A. Zaitsev, J. Rathousky, A. Zukal, M. Jančáková, *Appl. Catal.* 73 (1991) 65–81.
- [42] W. Wang, Y. Chen, *Appl. Catal.* 77 (1991) 223–233.
- [43] S. de Llobet, J.L. Pinilla, R. Moliner, I. Suelves, *Fuel* 139 (2015) 71–78.
- [44] R.T.K. Baker, M.A. Barber, P.S. Harris, F.S. Feates, R.J. Waite, *J. Catal.* 26 (1972) 51–62.
- [45] T. Baird, J.R. Fryer, B. Grant, *Carbon* 12 (1974) 591–602.
- [46] A. Oberlin, M. Endo, T. Koyama, *J. Cryst. Growth* 32 (1976) 335–349.
- [47] S.P. Gubin, Y.A. Koksharov, *Inorg. Mater.* 38 (2002) 1085–1099.
- [48] V.A. De La Peña O'Shea, P.R. De la Piscina, N. Hom, G. Aromí, J.L.G. Fierro, *Chem. Mater.* 21 (2009) 5637–5643.
- [49] J. Estephane, S. Aouad, S. Hany, B. El Khoury, C. Gennequin, H. El Zakhem, J. El Nakat, A. Aboukaïs, E. Abi Aad, *Int. J. Hydrol. Energy* 40 (2015) 9201–9208.
- [50] P.G. Harrison, I.K. Ball, W. Daniell, P. Lukinskas, M. Céspedes, E.E. Miró, M.A. Ulla, *Chem. Eng. J. (Lausanne)* 95 (2003) 47–55.
- [51] J. Liu, Z. Zhao, J. Wang, C. Xu, A. Duan, G. Jiang, Q. Yang, *Appl. Catal. B* 84 (2008) 185–195.